Article

Discovery Medicine 2025; 37(202): 2731–2743
https://doi.org/10.24976/Discov.Med.202537202.228

Fluorofenidone Attenuates Silica-Induced Pulmonary Fibrosis: Insights Into Its Mechanism of Action

Lujuan He[1], Jinyang Wu[2], Zezhi Zhou[1], Jing Long[1], Shenggang Liu[1,*]

[1]Department of Respiratory and Critical Care Medicine, The Affiliated Changsha Central Hospital, Hengyang Medical School, University of South China, 410007 Changsha, Hunan, China
[2]Department of Internal Neurology, The Affiliated Changsha Central Hospital, Hengyang Medical School, University of South China, 410007 Changsha, Hunan, China
*Correspondence: 2018050507@USC.edu.cn (Shenggang Liu)
Submitted: 1 September 2025 Revised: 23 October 2025 Accepted: 28 October 2025 Published: 20 November 2025

Background: Silicosis is a chronic, irreversible occupational pulmonary disorder characterized by persistent inflammation and fibrotic remodeling, with endoplasmic reticulum (ER) stress implicated in its pathogenesis. Fluorofenidone (AKF-PD), an anti-fibrotic agent, has shown protective properties in pulmonary fibrosis. This study aimed to evaluate the therapeutic effects of AKF-PD on silica-induced pulmonary fibrosis and elucidate its underlying molecular mechanisms.

Methods: A murine silicosis model was established through intratracheal instillation of a silica suspension. Mice were randomly divided into three groups: control, silica, or silica + AKF-PD (24 mice per group). Lung tissues were collected at 7, 14, and 28 days for histopathological analysis (hematoxylin and eosin (HE) and Masson staining), inflammation and fibrosis scoring, enzyme-linked immunosorbent assay (ELISA), reverse transcription quantitative real-time PCR (RT-qPCR), and western blotting. *In vitro*, MLE-12 cells were treated with silica in the presence or absence of AKF-PD or the ER stress inhibitor 4-PBA (4-PBA). Oxidative stress indices (malondialdehyde (MDA), reactive oxygen species (ROS), superoxide dismutase (SOD), glutathione (GSH)), inflammatory cytokines (interleukin (IL)-6, IL-1β), fibrosis markers (α-SMA, Fibronectin 1, Collagen IV), and ER stress-related proteins (Grp78, Chop, Xbp1, phospho-Ire1a, phospho-Eif2a) were quantified.

Results: *In vivo*, AKF-PD significantly attenuated alveolitis and fibrosis scores compared with the silica group, with Masson staining confirming reduced collagen deposition ($p < 0.001$). ELISA and RT-qPCR analyses showed decreased IL-6 (*Il6*) and IL-1β (*Il1b*) expression, while western blotting revealed downregulation of α-SMA, Fibronectin 1, and Collagen IV. ER stress markers (Grp78, Chop, Xbp1, phospho-Ire1a, phospho-Eif2a) and oxidative stress indices (MDA, ROS) were suppressed, accompanied by elevated GSH levels and SOD activity ($p < 0.05$). *In vitro*, AKF-PD reduced silica-induced production of inflammatory cytokines, fibrotic proteins, and ER stress mediators in MLE-12 cells ($p < 0.05$). These effects were comparable to those of 4-PBA, indicating that modulation of ER stress and oxidative stress contributed to the observed protection.

Conclusions: AKF-PD alleviates silica-induced pulmonary inflammation and fibrosis *in vivo* and *in vitro*. Its protective effects are associated with the regulation of ER stress and oxidative stress pathways, highlighting AKF-PD as a promising therapeutic candidate for silicosis.

Keywords: fluorofenidone; silicosis fibrosis; endoplasmic reticulum stress

Introduction

Silicosis is an occupational lung disorder that results from prolonged exposure to silica particles and their accumulation within the lungs during occupational exposure [1]. The pathological manifestations of silicosis are characterized by diffuse alveolitis in the early stage and irreversible pulmonary fibrosis in the later stage [2]. To date, no effective therapy has been established for silicosis, and it remains one of the most pressing occupational health and safety challenges in China. Consequently, elucidating the mechanisms underlying the onset and progression of silicosis and identifying effective therapeutic agents are considered both critical and urgent tasks.

Endoplasmic reticulum (ER) stress represents a cellular adaptive response to abnormal protein folding in the ER under adverse environmental conditions [3]. Previous studies have demonstrated that ER stress levels are significantly elevated in pulmonary fibrosis and play a pivotal role in disease progression [4,5], suggesting that modulation of ER stress may represent a potential therapeutic approach.

Fluorofenidone (AKF-PD), a novel pyridone derivative independently developed by our research group, exhibits anti-inflammatory, antioxidant, and anti-fibrotic properties and has demonstrated therapeutic benefits in multiple fibrotic conditions, including hepatic [6], renal [7], and pulmonary fibrosis [8]. Despite these advances, the

specific role of AKF-PD in silicosis-related fibrosis has not yet been elucidated.

In the present study, we established both an *in vivo* murine model of silicosis and an *in vitro* mouse alveolar epithelial cell model of silica-induced injury, followed by intervention with AKF-PD. Through integrated histopathological and molecular biological analyses, we aimed to evaluate the protective effects of AKF-PD and elucidate its underlying mechanisms. The findings are expected to provide an experimental foundation for developing novel preventive and therapeutic approaches for silicosis.

Materials and Methods

Animals Models

Seventy-two male C57BL/6 mice (6–8 weeks old, 20–25 g; Hunan Slake Jingda Experimental Animal Co., Ltd., Changsha, China) were purchased and housed under standardized housing conditions (23 °C, 45%–50% relative humidity, 12 h light/dark cycle) with *ad libitum* access to food and water. Following a one-week acclimation period, the mice were randomly assigned to three groups (n = 24 mice/group). All experimental protocols were reviewed and approved by the Animal Ethics Committee of University of South China (approval no. 2021-S0173).

Animal Grouping and Treatment

The mice were randomly divided into three groups: control, silicosis model, and AKF-PD treatment (24 mice each). The silicosis model was established by intratracheal instillation of a silica suspension (Sigma-Aldrich, St. Louis, MO, USA; S5631) at a concentration of 200 mg/mL and a dosage of 200 mg/kg, as previously described [9]. The control group received an equal volume of sterile saline through the trachea, while the remaining groups were administered the pre-prepared silica dust suspension through the trachea.

At 24 hours post-instillation, the AKF-PD treatment group received AKF-PD (Yichang Changjiang Pharmaceutical Co., Ltd., Yichang, China; purity ≥98%) via oral gavage at 500 mg/kg/day, as previously described [8]. The other groups received an equal volume of saline.

At each experimental time point (7, 14, and 28 days of continuous administration), eight mice per group were euthanized via intraperitoneal injection of pentobarbital sodium at an overdose concentration (150 mg/kg), and lung tissue samples were collected. The left lungs were fixed in 10% neutral buffered formalin solution for pathological analysis, while the right lungs were immediately snap-frozen in liquid nitrogen and stored for subsequent RNA and protein extraction.

Hematoxylin and Eosin (HE) and Masson Staining

Lung tissues were processed through standard dehydration, paraffin embedding, and sectioning procedures, followed by hematoxylin and eosin (HE) staining (Beyotime Biotechnology, Shanghai, China; C0105S) and Masson's trichrome staining (Solarbio Life Sciences, Beijing, China; G1340). Morphological alterations were examined under a light microscope (Olympus BX53, Tokyo, Japan). Alveolar inflammation and pulmonary fibrosis were scored according to established histopathological criteria [10,11].

Cell Grouping and Treatment

Mouse type II alveolar epithelial cells (MLE-12, ATCC® CRL-2110™, Manassas, VA, USA) were cultured in DMEM/F12 medium (Gibco, Thermo Fisher Scientific, Waltham, MA, USA; 11320033) supplemented with 10% fetal bovine serum (FBS; Gibco; A5669701) and 1% penicillin-streptomycin (Gibco; 15140122) at 37 °C in a humidified incubator with 5% CO_2. The MLE-12 cell line was authenticated by short tandem repeat (STR) profiling before use, and routine screening confirmed the absence of mycoplasma contamination.

The cells were randomly assigned into four groups: (1) normal control; (2) silica stimulation (50 μg/mL) [8,12,13]; (3) silica + AKF-PD treatment (400 mg/L); and (4) silica + 4-PBA treatment (0.5 mmol/L, Sigma-Aldrich; P21005).

Oxidative Stress Assays

Oxidative stress levels in lung tissues and MLE-12 cells were determined using standard biochemical assays. Malondialdehyde (MDA) content, an indicator of lipid peroxidation, was quantified using a lipid peroxidation assay kit (Nanjing Jiancheng Bioengineering Institute, Nanjing, China; A003-2). Superoxide dismutase (SOD) activity, reflecting antioxidant capacity, was determined using a SOD activity assay kit (Nanjing Jiancheng Bioengineering; A001-3), and glutathione (GSH) levels were measured using a GSH assay kit (Nanjing Jiancheng Bioengineering; A006-2). Intracellular reactive oxygen species (ROS) was detected with the fluorescent probe DCFH-DA (Beyotime Biotechnology, Shanghai, China; S0034) following the manufacturer's instructions, and fluorescence intensity was measured using a microplate reader (BioTek Synergy H1, Winooski, VT, USA).

Enzyme-Linked Immunosorbent Assay (ELISA)

Protein levels of IL-6 and IL-1β in lung tissue homogenates and MLE-12 cell culture supernatants were quantified using commercial mouse ELISA kits (R&D Systems, Minneapolis, MN, USA; IL-6 M6000B, IL-1β MLB00C) according to the manufacturer's instructions. Briefly, standards and samples were added to pre-coated plates and incubated with specific detection antibodies, followed by HRP-conjugated secondary antibodies. The colorimetric reaction was developed using TMB substrate, and absorbance was measured at 450 nm with a microplate reader (BioTek Synergy H1, Winooski, VT, USA). Cy-

tokine concentrations were normalized to total protein content in tissue extracts and presented as picograms per milligram of protein.

Western Blotting

Lung tissue and MLE-12 cells were lysed in RIPA buffer (Beyotime Biotechnology, Shanghai, China; P0013) supplemented with protease and phosphatase inhibitor cocktails. Protein extracts (30–50 µg) were separated on 10–12% SDS-PAGE gels and transferred onto polyvinylidene difluoride (PVDF) membranes (Millipore, Billerica, MA, USA). The membranes were blocked with TBST containing 5% non-fat milk for 1 h at room temperature, followed by overnight incubation at 4 °C with primary antibodies against Collagen IV (Abways, Shanghai, China; CY1657; 1:1000), Fibronectin 1 (Abways; CY9537; 1:2000), Grp78 (Abways; CY5166; 1:2000), Chop (Abways; CY6694; 1:2000), Xbp1 (Abways; CY6725; 1:2000), phospho-Ire1a (Abcam, Cambridge, UK; ab48187; 1:2000), Ire1a (Abcam; ab37073; 1:1000), phospho-Eif2a (Abways; CY5036; 1:1000), Eif2a (Abways; AB3335; 1:1000), α-SMA (Proteintech, Wuhan, China; 14395-1-AP; 1:1000), and Gapdh (Sigma-Aldrich; G9545; 1:5000).

After washing, membranes were incubated with HRP-labeled secondary antibodies (Cell Signaling Technology, Danvers, MA, USA; #7074, anti-rabbit IgG; 1:3000, and #7076, anti-mouse IgG; 1:3000) for 1 h at room temperature. The anti-mouse secondary antibody (#7076) was used to detect the mouse-derived Eif2a primary antibody, whereas #7074 was used for all rabbit-derived primary antibodies. Protein bands were visualized using an enhanced chemiluminescence detection system (ECL; Thermo Fisher Scientific, Waltham, MA, USA) and quantified using ImageJ software (NIH, Bethesda, MD, USA).

Reverse Transcription Quantitative Real-Time PCR (RT-qPCR)

Total RNA was extracted from lung tissues and MLE-12 cells using TRIzol reagent (Invitrogen, Carlsbad, CA, USA; 15596018CN) following the manufacturer's instructions. RNA concentration and purity were determined using a NanoDrop 2000 spectrophotometer (Thermo Fisher Scientific). Complementary DNA (cDNA) was synthesized using the HiScript III RT SuperMix kit (Vazyme, Nanjing, China; R323). Quantitative PCR (qPCR) was performed on a StepOnePlus Real-Time PCR System (Applied Biosystems, Foster City, CA, USA) with SYBR Green Master Mix (Vazyme; Q311). *Actb* (encoding β-actin) served as the internal reference gene. Relative mRNA expression levels were calculated using the $2^{-\Delta\Delta Ct}$ method. Primer sequences for *Col4a1* (encoding Collagen IV), *Fn1* (encoding Fibronectin 1), *Acta2* (encoding α-SMA), *Hspa5* (encoding Grp78), *Chop*, *Xbp1*, *Il6*, and *Il1b* are listed in Table 1.

Statistical Analysis

All experiments were conducted independently at least three times, and data are expressed as mean $\pm$ standard deviation (SD). Normality and homogeneity of variance were evaluated before statistical analysis. One-way analysis of variance (ANOVA) was performed, followed by Tukey's post hoc analysis for multiple comparisons. Statistical analyses were conducted using SPSS software (version 19.0; IBM, Armonk, NY, USA), and data visualization was performed using GraphPad Prism (version 8.0; GraphPad Software Inc., San Diego, CA, USA). A p-value < 0.5 was considered statistically significant.

Table 1. Primer sequences used for quantitative RT-qPCR analysis.

Gene (*Mus*)	Primer	Sequence (5′-3′)	Product size (bp)
Actb	F	CATTGCTGACAGGATGCAGAAGG	138
	R	TGCTGGAAGGTGGACAGTGAGG	
Col4a1	F	ATAAAGGTGACGTTGGGCTT	130
	R	CGGGAACCTTTATCACCAGTG	
Fn1	F	TTGTTCGGTGGAGTAGACCC	220
	R	GTGCCAGTGGTCTCTTGTTG	
Xbp1	F	AAAACAGAGTAGCAGCGCAG	183
	R	CCATTCCCAAGCGTGTTCTT	
Chop	F	TCACTACTCTTGACCCTGCG	174
	R	ACTGACCACTCTGTTTCCGT	
Hspa5	F	TCTCAGATCTTCTCCACGGC	202
	R	CTTCAGCTGTCACTCGGAGA	
Acta2	F	CTTCGCTGGTGATGATGCTC	175
	R	GTTGGTGATGATGCCGTGTT	
Il6	F	TACCACTTCACAAGTCGGAGGC	116
	R	CTGCAAGTGCATCATCGTTGTTC	
Il1b	F	TGGACCTTCCAGGATGAGGACA	148
	R	GTTCATCTCGGAGCCTGTAGTG	

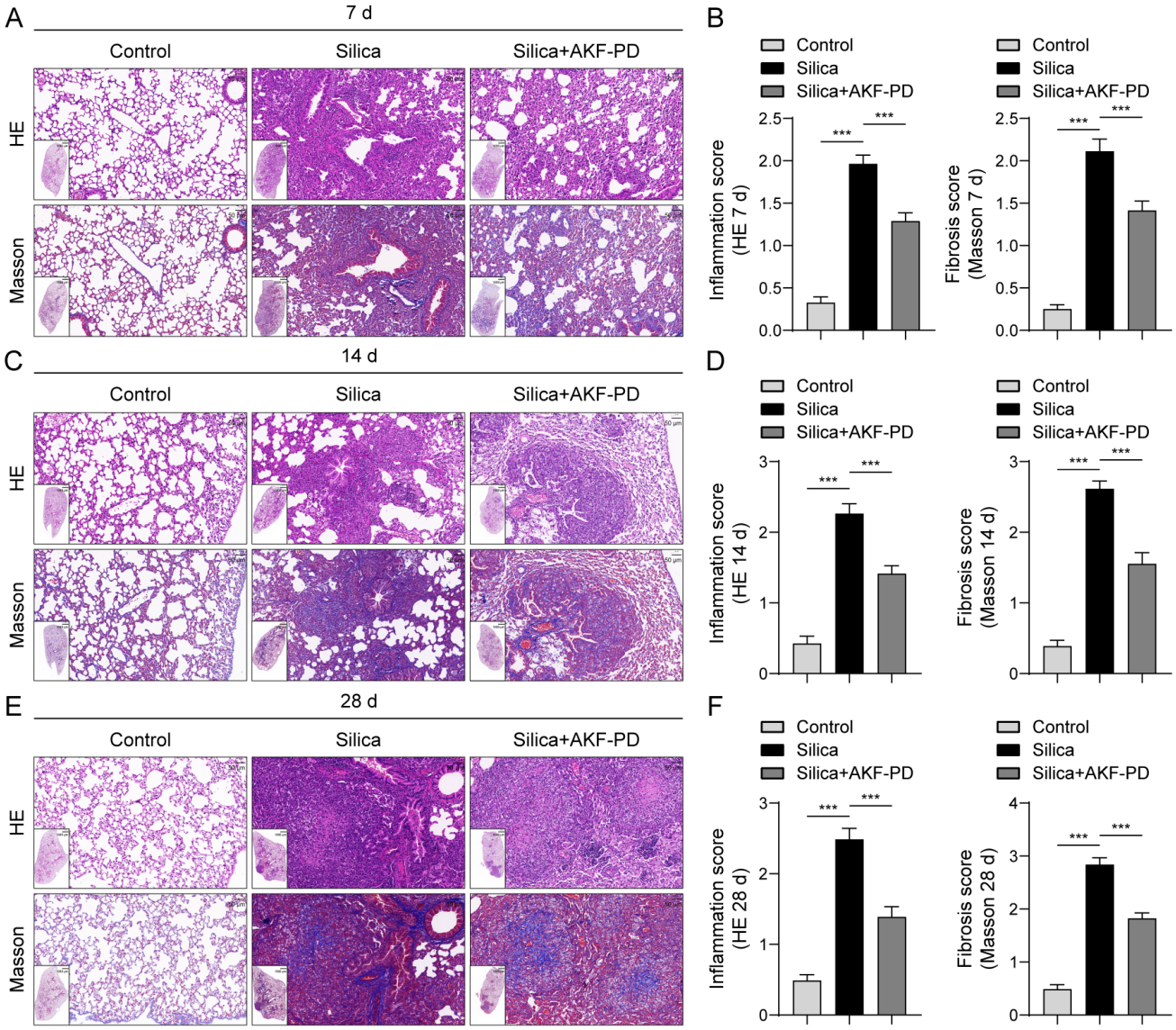

Fig. 1. AKF-PD attenuates silica-induced pulmonary inflammation and fibrosis. Mice received intratracheal instillation of silica followed by AKF-PD treatment and were euthanized at 7, 14, or 28 days post-exposure. Lung sections were subjected to HE staining for histopathological evaluation and Masson's trichrome staining for collagen assessment. (A,C,E) Representative HE and Masson's trichrome images of lung sections at 7 (A), 14 (C), and 28 (E) days after silica exposure. (B,D,F) Quantitative inflammation and fibrosis scores of lung tissues at the corresponding time points. n = 8, ***$p < 0.001$. AKF-PD, Fluorofenidone; HE, hematoxylin and eosin.

Results

AKF-PD Alleviates Silica-Induced Pathological Lung Injury in Mice

The effects of AKF-PD on silica-induced pulmonary inflammation and fibrosis were evaluated by HE and Masson's trichrome staining of lung tissue sections. In the control group, lung histology remained essentially normal at days 7, 14, and 28 (Fig. 1A,C,E), showing intact alveolar structures without inflammatory cell infiltration. In contrast, the silicosis model group exhibited marked pathological alterations following silica instillation. After 7 days, a large number of inflammatory cells infiltrated the lung parenchyma, and macrophages were observed within the alveolar cavities. Small, discrete cellular nodules primarily composed of macrophages were evident (Fig. 1A). By 14 days, multiple cellular nodules had formed, with some showing partial fusion. As exposure time increased, alveolar septa became markedly thickened, and both the number and size of cellular nodules further increased (Fig. 1C). By 28 days, extensive confluent nodules were observed, accompanied by significant collagen fiber deposition, resulting in the formation of cellular fibrous nodules (Fig. 1E).

Masson's trichome staining corroborated these findings. Collagen accumulation, indicated by blue-purple staining, progressively increased in the fibrotic regions

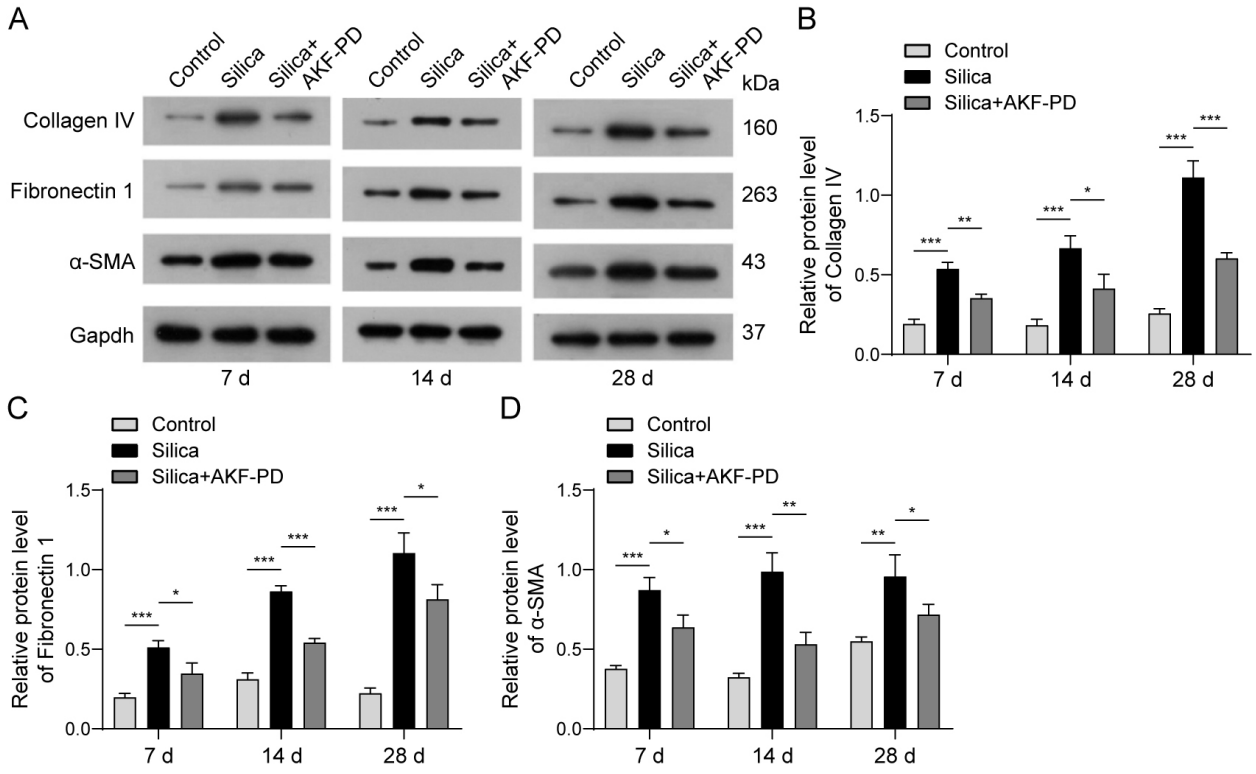

Fig. 2. AKF-PD suppresses silica-induced fibrotic protein expression. (A) Representative western blots of Collagen IV, Fibronectin 1, and α-SMA. (B–D) Densitometric quantification of Collagen IV (B), Fibronectin 1 (C), and α-SMA (D) relative to Gapdh. n = 3, *$p < 0.05$, **$p < 0.01$, ***$p < 0.001$.

with prolonged silica exposure, reflecting extracellular matrix (ECM) buildup and fibrosis progression. Notably, AKF-PD treatment markedly reduced inflammatory cell infiltration, alveolar septal thickening, and collagen deposition at all examined time points compared with the silica group (Fig. 1A,C,E). Histopathological scores (Fig. 1B,D,F) demonstrated that silica exposure significantly elevated both alveolitis and fibrosis scores compared with controls ($p < 0.001$, depending on time point), whereas AKF-PD treatment significantly reduced these scores relative to the silica group ($p < 0.001$).

AKF-PD Reduces Silica-Induced Pulmonary Fibrosis Markers

To investigate the effects of AKF-PD on silica-induced pulmonary fibrosis, the expression of fibrosis-associated proteins in mouse lung tissues was analyzed at 7, 14, and 28 days post-silica instillation. The western blot revealed that Collagen IV, Fibronectin 1, and α-SMA were significantly upregulated in the silica group compared with the control group. These increases became more evident with prolonged silica exposure, reflecting progressive fibrotic remodeling. Treatment with AKF-PD markedly attenuated the expression of these fibrosis-associated proteins at all time points compared with the silica group ($p < 0.01$, Fig. 2A). Quantitative densitometric analysis further confirmed that Collagen IV, Fibronectin 1, and α-SMA (Fig. 2B–D) levels were significantly lower in the lung tissues of AKF-PD-treated mice compared with silica-exposed mice ($p < 0.05$). Collectively, these observations suggest that AKF-PD effectively suppresses silica-induced fibrotic protein expression and mitigates pathological lung remodeling.

AKF-PD Decreases Silica-Induced Inflammatory Cytokine Levels and Oxidative Stress in Lung Tissue

Chronic pulmonary inflammation is a major contributor to fibrosis and is closely associated with pro-inflammatory cytokines such as IL-6 and IL-1β [14]. To assess whether AKF-PD modulates silica-induced pulmonary inflammation, the mRNA and protein levels of IL-6 (*Il6*) and IL-1β (*Il1b*) in lung tissues were quantified by RT-qPCR and ELISA at 7-, 14-, and 28- days post-exposure. In the silica group, IL-6 (*Il6*) mRNA and protein levels were significantly elevated compared with controls at all examined time points ($p < 0.001$, Fig. 3A,C). Similarly, IL-1β levels were markedly increased at 7, 14, and 28 days ($p < 0.001$, Fig. 3B,D). Treatment with AKF-PD significantly attenuated the silica-induced elevations of both IL-6 and IL-1β across all time points ($p < 0.01$, Fig. 3A–D). These findings indicate that AKF-PD exerts potent anti-inflammatory effects *in vivo* by downregulating silica-induced cytokine production in lung tissue.

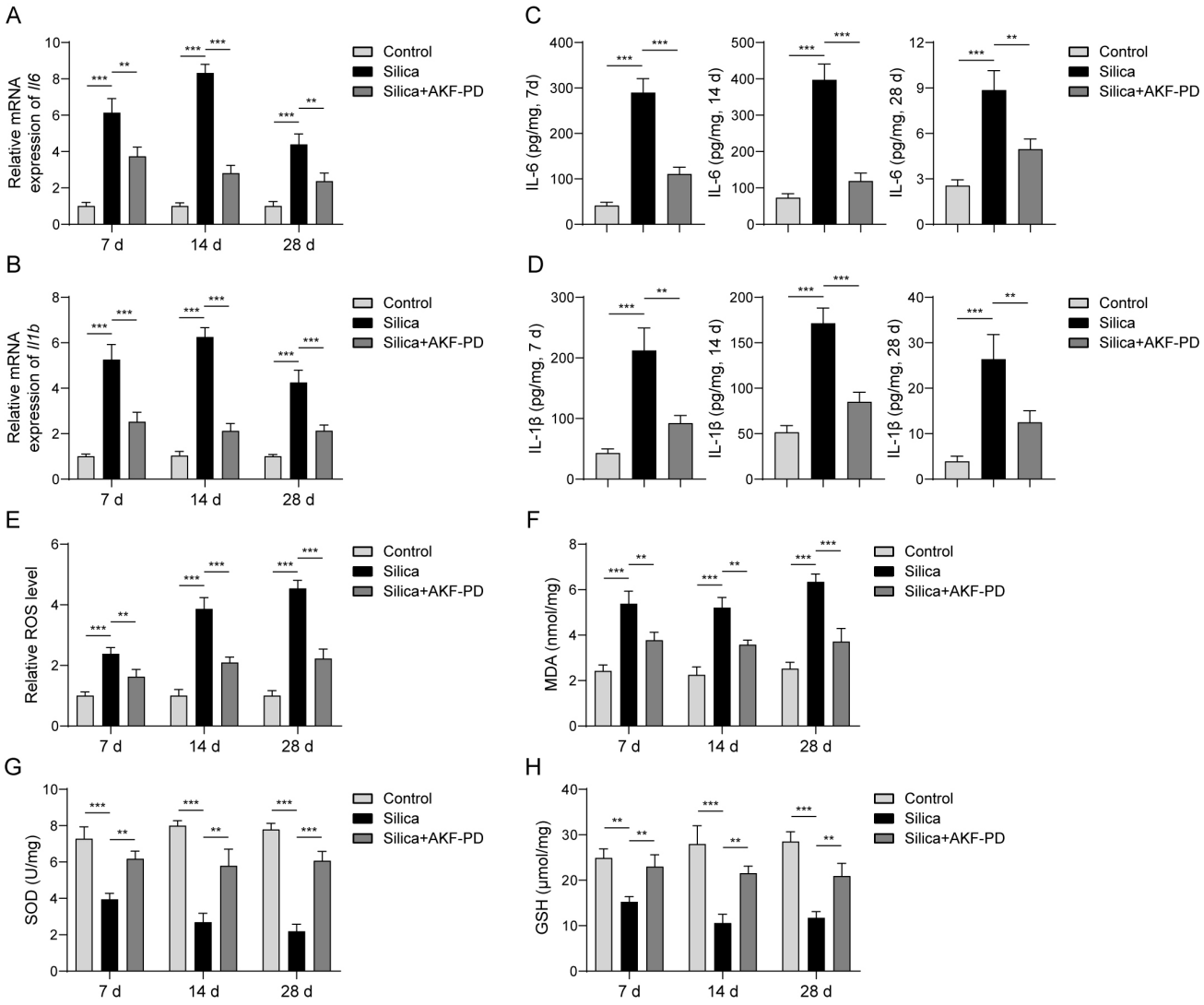

Fig. 3. AKF-PD mitigates silica-induced inflammatory and oxidative stress responses. The mRNA and protein levels of IL-6 (*Il6)* and IL-1β (*Il1b)* in lung tissue were determined by RT-qPCR and ELISA, respectively. (A,B) Relative *Il6* and I*l1b* mRNA levels at 7, 14, and 28 days. (C,D) Corresponding protein levels of IL-6 and IL-1β. Oxidative stress indicators were also assessed: (E) ROS levels, (F) MDA levels, (G) SOD activity, and (H) GSH activity in lung tissues at 7, 14, and 28 days. n = 3, $^{**}p < 0.01$, $^{***}p < 0.001$. RT-qPCR, reverse transcription quantitative real-time PCR; ELISA, enzyme-linked immunosorbent assay; ROS, reactive oxygen species; SOD, superoxide dismutase; GSH, glutathione; MDA, malondialdehyde.

To further evaluate the effects of AKF-PD on oxidative stress, oxidative stress markers in lung tissues were assessed at 7-, 14-, and 28- days post-exposure. In the silica group, ROS and MDA levels were significantly elevated, while SOD and GSH activities were markedly decreased compared with controls at all examined time points ($p < 0.01$, Fig. 3E–H). Treatment with AKF-PD significantly reduced ROS and MDA levels and restored SOD and GSH activities across all time points ($p < 0.01$, Fig. 3E–H). These results indicate that AKF-PD effectively alleviates silica-induced oxidative stress *in vivo*, thereby contributing to its protective role against lung injury.

AKF-PD Attenuates ER Stress in Silica-Exposed Mouse Lung Tissue

To further examine whether AKF-PD alleviates silica-related lung injury through regulation of ER stress, the expression of ER stress-related proteins was analyzed by western blotting at 7, 14, and 28 days. In the silicosis model group, protein levels of Grp78, Chop, Xbp1, phospho-Ire1a, and phospho-Eif2a were significantly upregulated compared with those in the control group ($p < 0.01$, Fig. 4A–F), indicating activation of ER stress pathways. Treatment with AKF-PD markedly inhibited the silica-induced upregulation of these proteins at all examined time points ($p < 0.05$, Fig. 4A–F), suggesting that AKF-PD effectively attenuates ER stress signaling. These

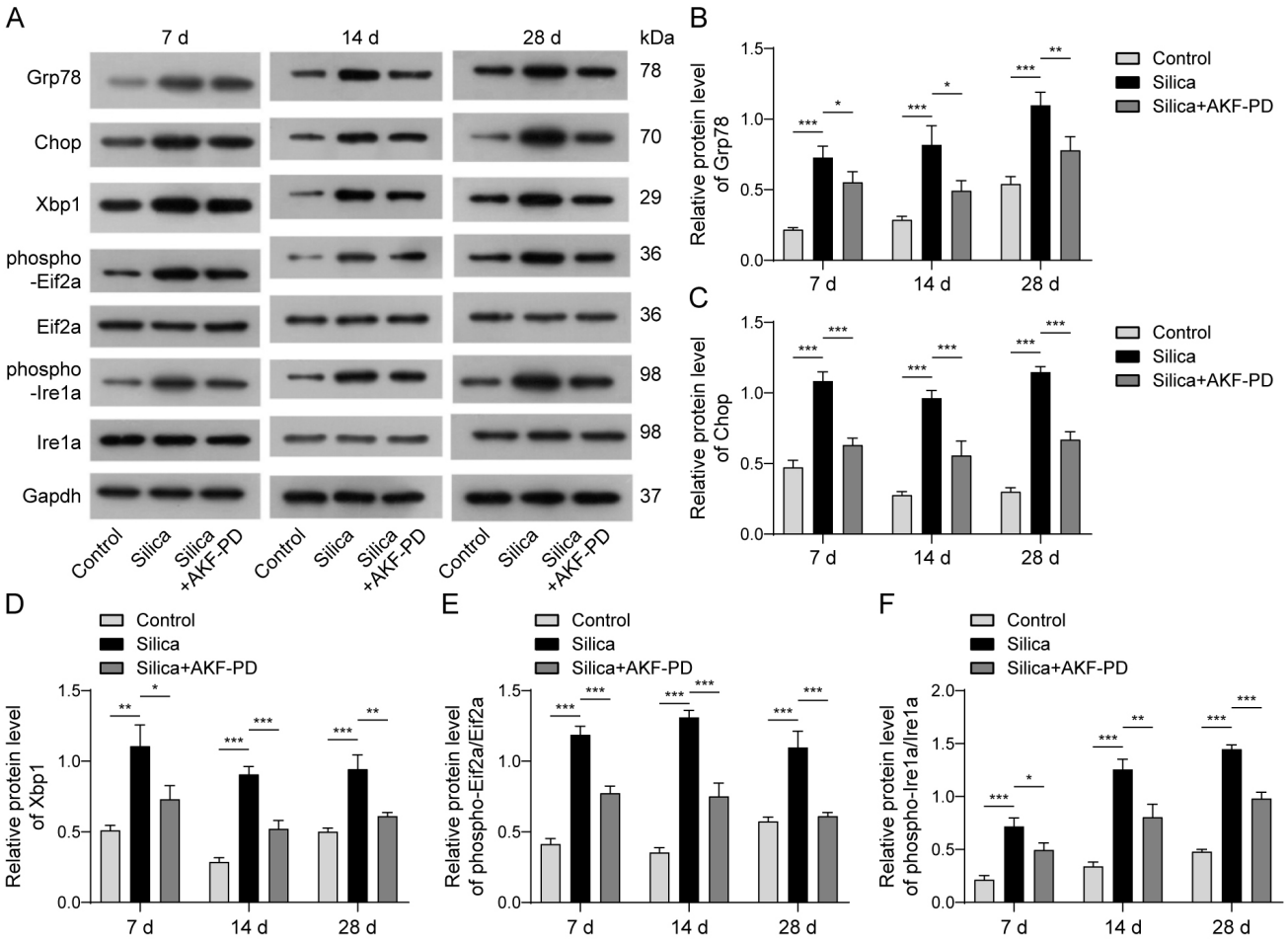

Fig. 4. AKF-PD attenuates ER stress in silica-exposed mouse lung tissue. (A) Representative western blots of Grp78, Chop, Xbp1, phospho-Eif2a, Eif2a, phospho-Ire1a, Ire1a, and Gapdh expression. (B–F) Quantitative analyses of Grp78 (B), Chop (C), Xbp1 (D), phospho-Eif2a/Eif2a (E), and phospho-Ire1a/Ire1a (F) ratios. n = 3, *$p < 0.05$, **$p < 0.01$, ***$p < 0.001$.

findings demonstrate that AKF-PD mitigates silica-induced ER stress responses in lung tissue, which may contribute to its observed anti-inflammatory and anti-fibrotic effects in the silicosis model.

AKF-PD Suppresses Inflammatory Responses and Oxidative Stress in Silica-Stimulated MLE-12 Cells

To investigate the cellular mechanisms of AKF-PD, MLE-12 cells were used for *in vitro* experiments. Following silica exposure, cells secreted significantly higher levels of the pro-inflammatory cytokines IL-6 and IL-1β, accompanied by enhanced oxidative stress, as indicated by elevated ROS and MDA levels and decreased SOD and GSH activities compared with controls ($p < 0.001$, Fig. 5A–H). Treatment with AKF-PD significantly reduced IL-6 and IL-1β expression and restored oxidative stress markers, yielding results comparable to those achieved with 4-PBA, a known ER stress inhibitor ($p < 0.01$ versus silica group, Fig. 5A–H). These findings suggest that AKF-PD exerts protective effects against silica-induced injury in alveolar epithelial cells by attenuating both inflammatory cytokine release and oxidative stress, likely through modulation of ER stress-related signaling pathways.

AKF-PD Reduces Fibrotic Protein Expression in Silica-Stimulated MLE-12 Cells

To further explore the impact of AKF-PD on fibrotic responses in MLE-12 cells, fibrosis-associated protein expression was evaluated after silica stimulation. Western blotting analysis revealed that silica exposure significantly elevated the levels of Collagen IV, Fibronectin 1, and α-SMA compared with controls ($p < 0.001$, Fig. 6A–D). Treatment with AKF-PD significantly suppressed the upregulation of these fibrotic markers, with effects similar to those of 4-PBA ($p < 0.01$, Fig. 6A–D). These findings indicate that AKF-PD mitigates silica-induced fibrotic responses in alveolar type II epithelial cells, consistent with its anti-fibrotic effects observed *in vivo*.

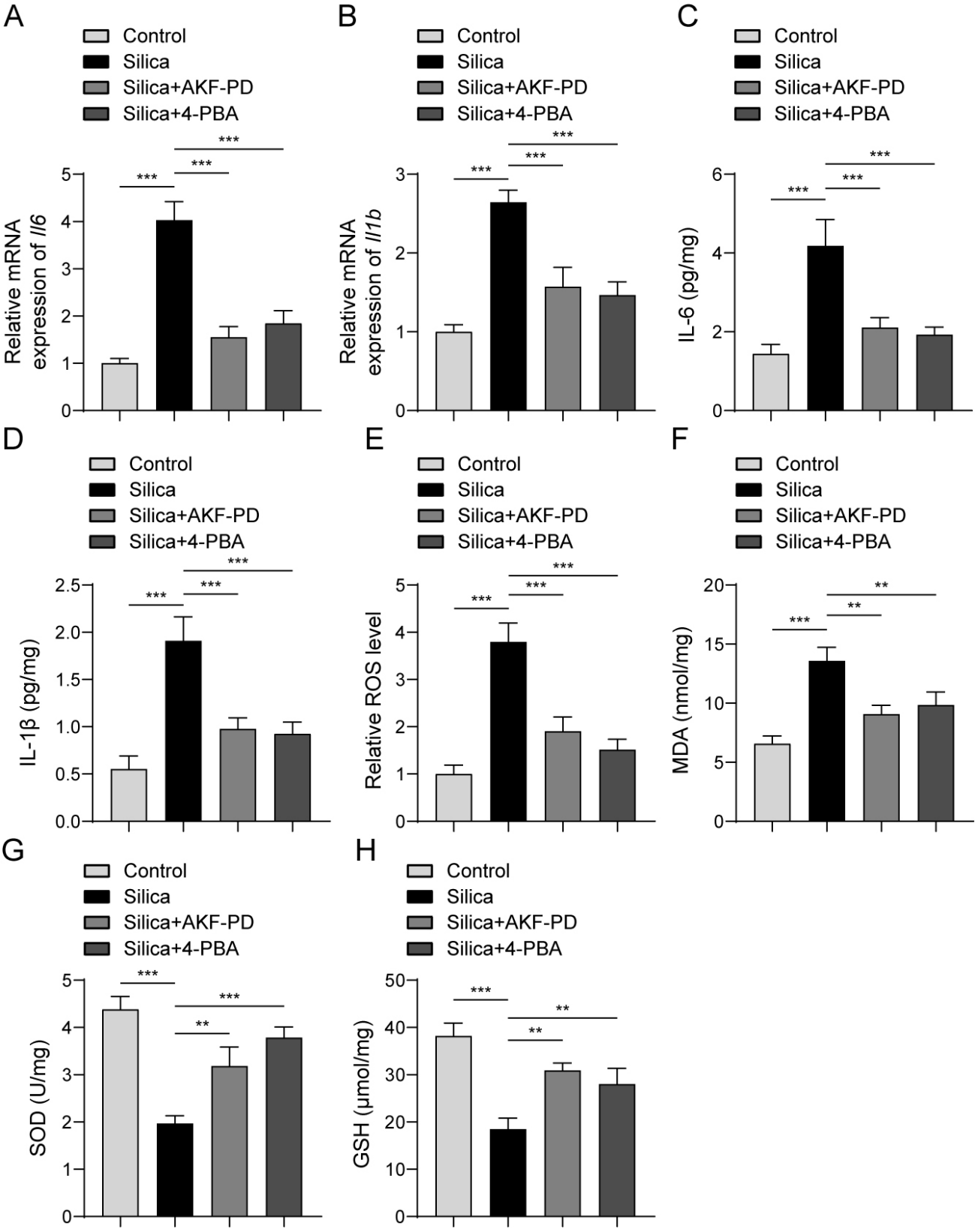

Fig. 5. AKF-PD attenuates silica-induced inflammatory cytokine expression and oxidative stress in MLE-12 cells. MLE-12 cells were exposed to silica (50 μg/mL) for 24 h, followed by treatment with AKF-PD (400 mg/L) or the ER stress inhibitor 4-PBA (0.5 mmol/L) for an additional 24 h. (A,B) Relative mRNA expression levels of *Il6* and *Il1b* determined by RT-qPCR. (C,D) IL-6 and IL-1β protein levels measured in cell supernatants by ELISA. (E–H) Oxidative stress indicators, including ROS, MDA, SOD activity, and GSH levels, were quantified in treated cells. n = 3, $^{**}p < 0.01$, $^{***}p < 0.001$.

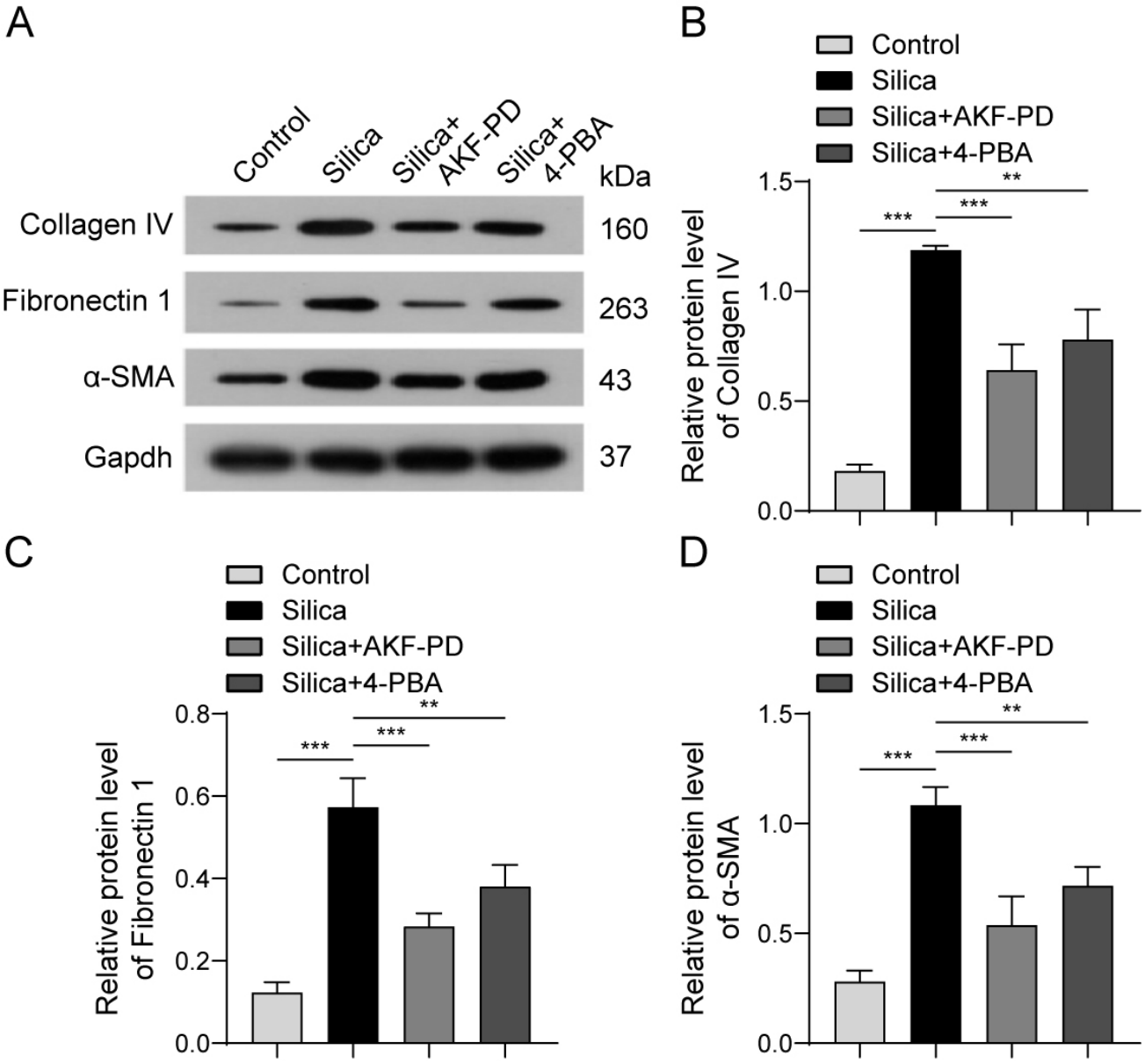

Fig. 6. AKF-PD reduces silica-induced fibrotic protein expression in MLE-12 cells. (A) Representative western blots of Collagen IV, Fibronectin 1, and α-SMA in each treatment group. (B–D) Densitometric quantification of Collagen IV (B), Fibronectin 1 (C), and α-SMA (D) normalized to Gapdh. n = 3, $^{**}p < 0.01$, $^{***}p < 0.001$.

AKF-PD Downregulates ER Stress Markers in Silica-Stimulated MLE-12 Cells

To further clarify the mechanism underlying the protective role of AKF-PD, its impact on ER stress was assessed *in vitro*. In MLE-12 cells, silica exposure markedly upregulated ER stress-related proteins, including Grp78, Chop, Xbp1, phospho-Ire1a, and phospho-Eif2a, compared with controls ($p < 0.001$, Fig. 7A–F). AKF-PD treatment significantly downregulated these proteins, producing effects comparable to those of 4-PBA ($p < 0.05$, Fig. 7A–F). These findings indicate that AKF-PD effectively alleviates silica-induced ER stress in alveolar type II epithelial cells.

AKF-PD Decreases Fibrosis- and ER Stress-Related mRNA Expression in MLE-12 Cells

To further confirm the regulatory role of AKF-PD on fibrosis and ER stress at the transcriptional level, we evaluated the mRNA expression of fibrosis- and ER stress-related genes in MLE-12 cells. Silica exposure significantly upregulated the mRNA expression of *Col4a1*, *Fn1*, and *Acta2*, as well as the ER stress markers *Hspa5*, *Chop*, and *Xbp1*, compared with the control group ($p < 0.001$, Fig. 8A–F). Treatment with AKF-PD markedly reduced the expression of these genes, and the effects were comparable to those of ER stress inhibitor 4-PBA ($p < 0.05$, Fig. 8A–F). These findings demonstrate that AKF-PD not only sup-

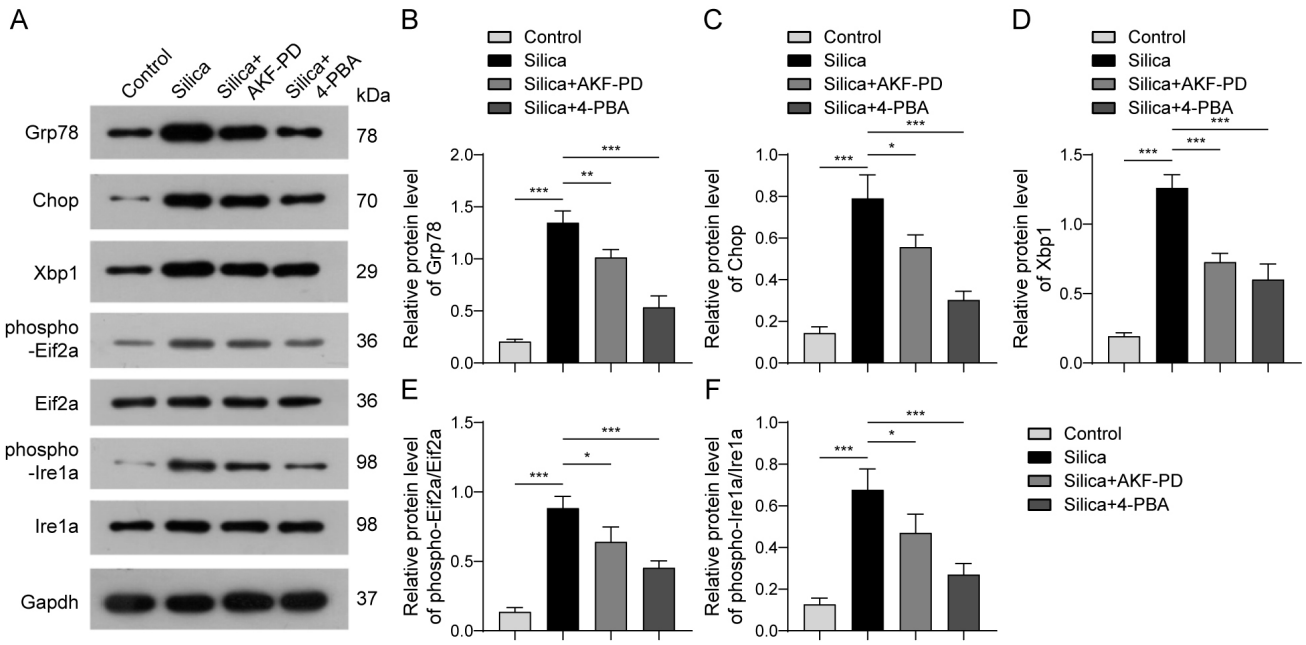

Fig. 7. AKF-PD attenuates silica-induced ER stress responses in MLE-12 cells. (A) Representative western blots of Grp78, Chop, Xbp1, phospho-Eif2a, Eif2a, phospho-Ire1a and Ire1a in each treatment group. (B–F) Quantitative analyses of Grp78 (B), Chop (C), Xbp1 (D), phospho-Eif2a/Eif2a (E), and phospho-Ire1a/Ire1a (F) ratios. n = 3, *$p < 0.05$, **$p < 0.01$, ***$p < 0.001$.

presses silica-induced protein expression but also downregulates the transcription of fibrosis- and ER stress-related genes, supporting its role in attenuating silica-induced cellular injury through modulation of the ER stress pathway.

Discussion

Silicosis is closely associated with both the concentration and duration of exposure to silica dust [15]. In humans, disease development is typically a chronic process characterized by a long latency period, with clinical symptoms often emerging only after 10–30 years of sustained exposure [16,17]. To better simulate the progression of human silicosis, we established a mouse model via intratracheal instillation of silica suspension and analyzed pathological changes at 1, 2, and 4 weeks post-exposure. Histopathological and molecular assessments demonstrated progressive pulmonary inflammation and fibrosis over time, thereby validating the model and providing a reliable platform for therapeutic evaluation.

Currently, therapeutic strategies for pulmonary fibrosis remain limited, highlighting the need to identify and develop novel pharmacological interventions. AKF-PD, a pyridone compound developed by our research team, has previously demonstrated potent anti-inflammatory and anti-fibrotic effects in models of hepatic, renal, and pulmonary fibrosis [6,8]. In this study, AKF-PD administration significantly attenuated silica-induced pulmonary injury. Histological evaluation (HE and Masson's staining) revealed decreased alveolitis and reduced collagen deposition in treated mice, while molecular assays (ELISA and western blotting) indicated lower levels of IL-1β, IL-6, Collagen IV, α-SMA, and Fibronectin 1. Collectively, these findings provide compelling evidence that AKF-PD exerts both anti-inflammatory and anti-fibrotic activities in the context of silicosis [18].

The ER, the organelle with the largest membrane surface area in eukaryotic cells, plays a central role in protein synthesis, folding, and quality control [19]. Disturbances in these processes can lead to the accumulation of misfolded proteins, triggering ER stress [20]. During the development of silicotic fibrosis, persistent ER stress induces apoptosis of alveolar type II epithelial cells, exacerbating tissue injury and promoting fibrotic remodeling [21]. Although the precise signaling mechanisms underlying ER stress-induced apoptosis remain under investigation, transcription factor-mediated and caspase-dependent signaling pathways are considered the principal routes involved.

In this study, AKF-PD was shown to modulate ER stress both *in vivo* and *in vitro*. In lung tissue, AKF-PD significantly downregulated the expression of Grp78, Chop, Xbp1, phospho-Ire1a, and phospho-Eif2a, accompanied by decreased levels of fibrotic markers (α-SMA, Fibronectin 1, and Collagen IV) at both the protein and mRNA levels. To further elucidate the underlying cellular mechanisms, we employed an *in vitro* model using MLE-12, which plays a pivotal role in silicosis pathogenesis. In this model, silica exposure markedly induced ER stress and fibrosis-related markers, while AKF-PD treatment significantly reduced their expression. Mechanistically, the capacity of AKF-PD to downregulate IRE1α phosphorylation is particularly sig-

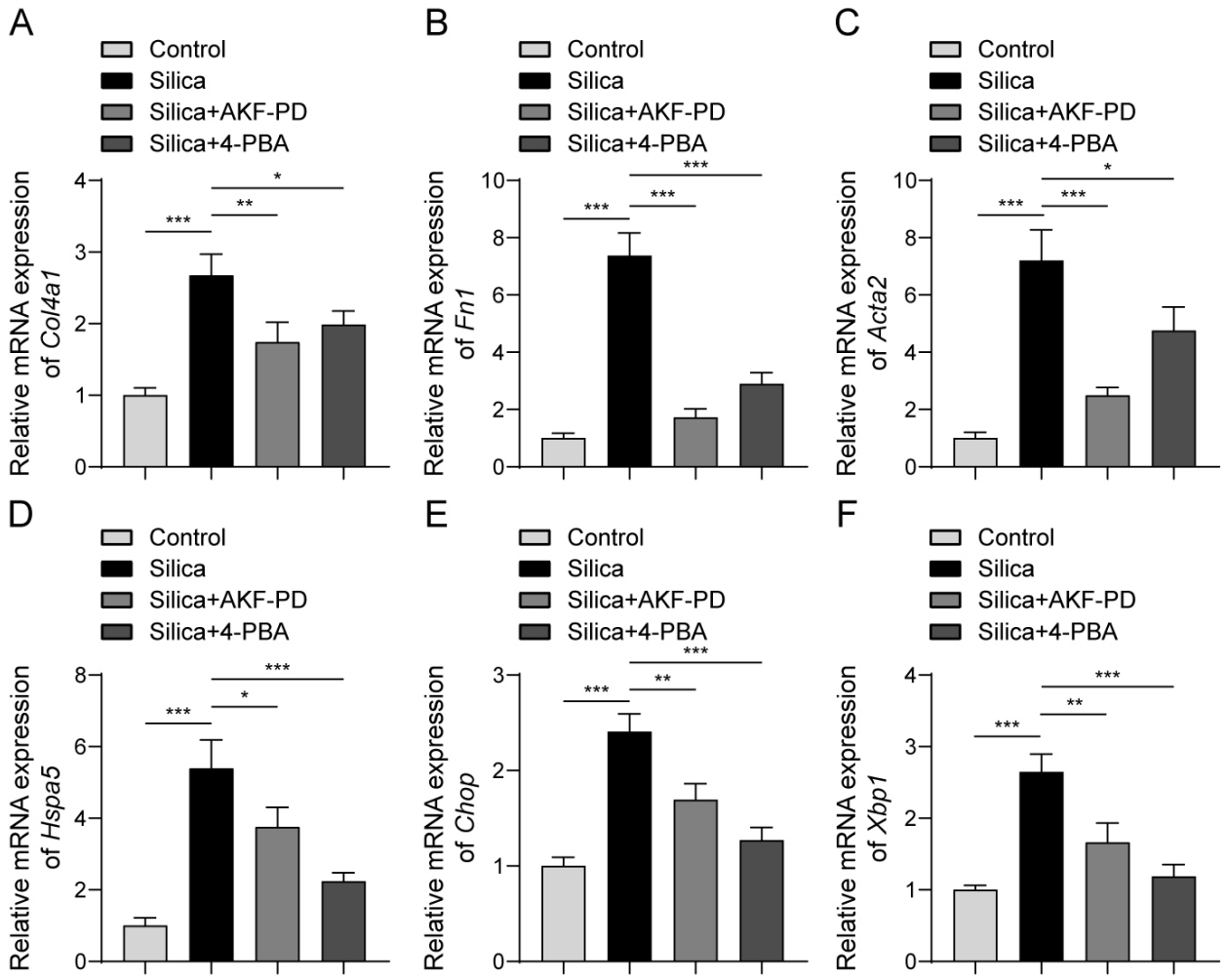

Fig. 8. AKF-PD decreases silica-induced expression of fibrosis- and ER stress-related genes in MLE-12 cells. Relative mRNA expression levels were measured by RT-qPCR following AKF-PD or 4-PBA treatment. Shown are expression levels of (A) *Col4a1*, (B) *Fn1*, (C) *Acta2*, (D) *Hspa5*, (E) *Chop*, and (F) *Xbp1*. n = 3, *$p < 0.05$, **$p < 0.01$, ***$p < 0.001$.

nificant. Given that the IRE1α–XBP1 signaling branch is central to unfolded protein response (UPR) activation and has been implicated in fibroblast activation and ECM deposition [22], our findings suggest that AKF-PD may mitigate fibrosis by preserving epithelial cell integrity and disrupting pro-fibrotic signaling cascades.

The inhibitory effects of AKF-PD were comparable to those of 4-PBA, a known ER stress inhibitor that has been shown to reduce α-SMA and collagen expression, and mitigate epithelial apoptosis [23]. Similarly, in silica-stimulated macrophage-derived exosome studies, 4-PBA pre-treatment reversed the upregulation of BiP, XBP1s, and phospho-eIF2α, and decreased fibrotic marker expression in lung tissue and bronchoalveolar lavage fluid (BALF) [24]. Our findings are consistent with these reports. The observation that AKF-PD and 4-PBA produce comparable reductions in UPR markers and fibrosis-associated proteins strengthens the concept that modulation of ER stress constitutes a core mechanism underlying the protective and anti-fibrotic effects of AKF-PD.

In addition to ER stress, oxidative stress represents another critical factor in the pathogenesis of silicosis and exhibits close mechanistic interplay with ER stress [25]. Our findings demonstrated that AKF-PD effectively attenuated oxidative stress, as evidenced by decreased levels of MDA and ROS, along with enhanced SOD activity. The concurrent suppression of oxidative and ER stress strongly suggests a dual regulatory mechanism through which AKF-PD confers cytoprotection by modulating both pathways [26]. Nevertheless, additional mechanistic studies are warranted to clarify the precise interplay between oxidative stress and ER stress during the progression of silicosis.

This study has several limitations. Although the sample size was adequate, it could be expanded to improve statistical power. Moreover, only a single high dose of AKF-PD was evaluated in one animal model and cell line, limiting dose-response assessment and generalizability. Furthermore, the short-term (28-day) observation period and exclusive focus on the ER stress pathway preclude insights into long-term effects and other potential mechanisms. Fu-

ture studies should address these limitations to comprehensively characterize the therapeutic potential of AKF-PD.

Conclusions

The present study demonstrates that AKF-PD effectively mitigates silica-induced pulmonary inflammation and fibrosis in both *in vivo* and *in vitro* models. Its protective effects are associated with the inhibition of ER stress and oxidative stress, leading to reduced alveolar epithelial damage and lower expression of fibrosis-related markers. Collectively, these findings suggest that AKF-PD is a promising therapeutic candidate for silicosis. However, further studies are required to validate its efficacy, determine optimal dosing regimens, and evaluate long-term safety.

Availability of Data and Materials

The datasets generated and/or analyzed during the current study are available from the corresponding author upon reasonable request.

Author Contributions

LH, SL conceived and designed the study. LH, JW performed the animal experiments and data collection. LH, ZZ carried out the cell culture assays and molecular analyses. LH, JW, ZZ, JL conducted statistical analysis. LH, JL, SL drafted the manuscript. All authors contributed to critical revision of the manuscript for important intellectual content. All authors read and approved the final manuscript. All authors have participated sufficiently in the work and agreed to be accountable for all aspects of the work.

Ethics Approval and Consent to Participate

All animal experimental procedures were reviewed and approved by the Experimental Animal Ethics Committee of University of South China (approval no. 2021-S0173). All procedures complied with the relevant guidelines for the care and use of laboratory animals.

Acknowledgment

The authors would like to thank the laboratory staff and department colleagues for their technical assistance and support during the course of this study.

Funding

This work was supported by the Natural Science Foundation of Changsha (Grant No. kq2202045) and the Natural Science Foundation of Hunan Province (Grant No. 2023JJ40071).

Conflict of Interest

The authors declare no conflict of interest.

References

[1] Wang D, Zhou M, Liu Y, Ma J, Yang M, Shi T, *et al*. Comparison of Risk of Silicosis in Metal Mines and Pottery Factories: A 44-Year Cohort Study. Chest. 2020; 158: 1050–1059. https://doi.org/10.1016/j.chest.2020.03.054.

[2] Li T, Yang X, Xu H, Liu H. Early Identification, Accurate Diagnosis, and Treatment of Silicosis. Canadian Respiratory Journal. 2022; 2022: 3769134. https://doi.org/10.1155/2022/3769134.

[3] Ye J, Liu X. Interactions between endoplasmic reticulum stress and extracellular vesicles in multiple diseases. Frontiers in Immunology. 2022; 13: 955419. https://doi.org/10.3389/fimmu.2022.955419.

[4] Borok Z, Horie M, Flodby P, Wang H, Liu Y, Ganesh S, *et al*. *Grp78* Loss in Epithelial Progenitors Reveals an Age-linked Role for Endoplasmic Reticulum Stress in Pulmonary Fibrosis. American Journal of Respiratory and Critical Care Medicine. 2020; 201: 198–211. https://doi.org/10.1164/rccm.201902-0451OC.

[5] Burman A, Tanjore H, Blackwell TS. Endoplasmic reticulum stress in pulmonary fibrosis. Matrix Biology. 2018; 68–69: 355–365. https://doi.org/10.1016/j.matbio.2018.03.015.

[6] Peng X, Yang H, Tao L, Xiao J, Zeng Y, Shen Y, *et al*. Fluorofenidone alleviates liver fibrosis by inhibiting hepatic stellate cell autophagy *via* the TGF-β1/Smad pathway: implications for liver cancer. PeerJ. 2023; 11: e16060. https://doi.org/10.7717/peerj.16060.

[7] Liao X, Lv X, Zhang Y, Han Y, Li J, Zeng J, *et al*. Fluorofenidone Inhibits UUO/IRI-Induced Renal Fibrosis by Reducing Mitochondrial Damage. Oxidative Medicine and Cellular Longevity. 2022; 2022: 2453617. https://doi.org/10.1155/2022/2453617.

[8] Song C, He L, Zhang J, Ma H, Yuan X, Hu G, *et al*. Fluorofenidone attenuates pulmonary inflammation and fibrosis via inhibiting the activation of NALP3 inflammasome and IL-1β/IL-1R1/MyD88/NF-κB pathway. Journal of Cellular and Molecular Medicine. 2016; 20: 2064–2077. https://doi.org/10.1111/jcmm.12898.

[9] He R, Yuan X, Lv X, Liu Q, Tao L, Meng J. Caveolin-1 negatively regulates inflammation and fibrosis in silicosis. Journal of Cellular and Molecular Medicine. 2022; 26: 99–107. https://doi.org/10.1111/jcmm.17045.

[10] Szapiel SV, Elson NA, Fulmer JD, Hunninghake GW, Crystal RG. Bleomycin-induced interstitial pulmonary disease in the nude, athymic mouse. The American Review of Respiratory Disease. 1979; 120: 893–899. https://doi.org/10.1164/arrd.1979.120.4.893.

[11] Ashcroft T, Simpson JM, Timbrell V. Simple method of estimating severity of pulmonary fibrosis on a numerical scale. Journal of Clinical Pathology. 1988; 41: 467–470. https://doi.org/10.1136/jcp.41.4.467.

[12] Jiang F, Li S, Jiang Y, Chen Z, Wang T, Liu W. Fluorofenidone attenuates paraquat induced pulmonary fibrosis by regulating the PI3K/Akt/mTOR signaling pathway and autophagy. Molecular Medicine Reports. 2021; 23: 405. https://doi.org/10.3892/mmr.2021.12044.

[13] Lv X, Yao T, He R, He Y, Li M, Han Y, *et al*. Protective Effect of Fluorofenidone Against Acute Lung Injury Through Suppressing the MAPK/NF-κB Pathway. Frontiers in Pharmacology. 2021; 12: 772031. https://doi.org/10.3389/fphar.2021.772031.

[14] Yin H, Fang L, Wang L, Xia Y, Tian J, Ma L, *et al*. Acute

Silica Exposure Triggers Pulmonary Inflammation Through Macrophage Pyroptosis: An Experimental Simulation. Frontiers in Immunology. 2022; 13: 874459. https://doi.org/10.3389/fimmu.2022.874459.

[15] Vanka KS, Shukla S, Gomez HM, James C, Palanisami T, Williams K, *et al*. Understanding the pathogenesis of occupational coal and silica dust-associated lung disease. European Respiratory Review. 2022; 31: 210250. https://doi.org/10.1183/16000617.0250-2021.

[16] Krefft S, Wolff J, Rose C. Silicosis: An Update and Guide for Clinicians. Clinics in Chest Medicine. 2020; 41: 709–722. https://doi.org/10.1016/j.ccm.2020.08.012.

[17] Song M, Wang J, Sun Y, Pang J, Li X, Liu Y, *et al*. Inhibition of gasdermin D-dependent pyroptosis attenuates the progression of silica-induced pulmonary inflammation and fibrosis. Acta Pharmaceutica Sinica. B. 2022; 12: 1213–1224. https://doi.org/10.1016/j.apsb.2021.10.006.

[18] Hassanein EHM, Ibrahim IM, Abd El-Maksoud MS, Abd El-Aziz MK, Abd-Alhameed EK, Althagafy HS. Targeting necroptosis in fibrosis. Molecular Biology Reports. 2023; 50: 10471–10484. https://doi.org/10.1007/s11033-023-08857-9.

[19] Wiseman RL, Mesgarzadeh JS, Hendershot LM. Reshaping endoplasmic reticulum quality control through the unfolded protein response. Molecular Cell. 2022; 82: 1477–1491. https://doi.org/10.1016/j.molcel.2022.03.025.

[20] Ren J, Bi Y, Sowers JR, Hetz C, Zhang Y. Endoplasmic reticulum stress and unfolded protein response in cardiovascular diseases. Nature Reviews. Cardiology. 2021; 18: 499–521. https://doi.org/10.1038/s41569-021-00511-w.

[21] Zhu W, Tan C, Zhang J. Alveolar Epithelial Type 2 Cell Dysfunction in Idiopathic Pulmonary Fibrosis. Lung. 2022; 200: 539–547. https://doi.org/10.1007/s00408-022-00571-w.

[22] Barabutis N. Unfolded Protein Response in Lung Health and Disease. Frontiers in Medicine. 2020; 7: 344. https://doi.org/10.3389/fmed.2020.00344.

[23] Hu YB, Wu X, Qin XF, Wang L, Pan PH. Role of Endoplasmic Reticulum Stress in Silica-induced Apoptosis in RAW264.7 Cells. Biomedical and Environmental Sciences. 2017; 30: 591–600. https://doi.org/10.3967/bes2017.078.

[24] Qin X, Lin X, Liu L, Li Y, Li X, Deng Z, *et al*. Macrophage-derived exosomes mediate silica-induced pulmonary fibrosis by activating fibroblast in an endoplasmic reticulum stress-dependent manner. Journal of Cellular and Molecular Medicine. 2021; 25: 4466–4477. https://doi.org/10.1111/jcmm.16524.

[25] Li S, Zhao J, Han G, Zhang X, Li N, Zhang Z. Silicon dioxide-induced endoplasmic reticulum stress of alveolar macrophages and its role on the formation of silicosis fibrosis: a review article. Toxicology Research. 2023; 12: 1024–1033. https://doi.org/10.1093/toxres/tfad099.

[26] Chen X, Shi C, He M, Xiong S, Xia X. Endoplasmic reticulum stress: molecular mechanism and therapeutic targets. Signal Transduction and Targeted Therapy. 2023; 8: 352. https://doi.org/10.1038/s41392-023-01570-w.